Tunable Oscillations in Optically Injected Semiconductor Lasers With Reduced Sensitivity to Perturbations

Thomas B. Simpson, Jia-Ming Liu, *Fellow, IEEE*, Mohammad AlMulla, Nicholas G. Usechak, *Senior Member, IEEE*, and Vassilios Kovanis

***Abstract*—Narrow linewidth optical injection into a semiconductor laser can induce periodic oscillations in the injected laser's output power with a frequency that is widely tunable by simply varying the steady-state bias current and operating temperature. Recently, it has been demonstrated that this oscillation frequency can be made nearly insensitive to small-signal fluctuations of these two parameters at certain operating points [1]. Here, we demonstrate that this insensitivity arises from multiwave mixing and interference that minimizes the response of both the gain medium and the circulating optical power at the oscillation frequency. Both experimental measurements and model calculations of optical spectra show that at the operating points of reduced oscillation frequency sensitivity, all strong components of the optical spectrum still exhibit a response to the perturbations. However, in the power spectra and the (calculated) carrier-density spectra, the response is strongly attenuated. Novel operating points that limit the sensitivity of the laser power oscillation frequency to perturbations offer the promise for improved operation of tunable photonic oscillators for radio- and microwave-frequency applications.**

***Index Terms*—Injection locking, RF Oscillators, tunable oscillators.**

I. Introduction

SEMICONDUCTOR lasers, due to their small size and fast dynamical characteristics, are of interest not only for their use in myriad applications, but also as a test medium to understand fundamental characteristics of laser systems distinct from the corrupting influence of temperature, mechanical and other extrinsic fluctuations [2], [3]. The injection-locking and dynamical-response characteristics of semiconductor lasers subject to injected optical signals has received considerable attention as a tool for the characterization of the intrinsic dynamic parameters of semiconductor lasers [4]–[8], and as a mechanism for enhancing the fundamental modulation characteristics [9]–[12], with applications in communications [13]–[16], RADAR [17], LIDAR [18], cryptography [19], random bit generation [20], and photonic frequency synthesis [21]–[24]. Under external injection, the semiconductor laser can be induced to display a broad range of output characteristics including stable injection locking, periodic power oscillations at the fundamental dynamic resonance frequency of the system and its subharmonics, and chaotic dynamics [25]–[27]. The specific output characteristics can be controlled simply by tuning the operating points of the laser through control of the operating temperature and dc-bias current. As these capabilities are understood, attention is shifting to quantifying and minimizing the effects of unwanted fluctuations in the operating point of the laser (the dc bias current and operating temperature) to the desired output characteristics [1], [23], [24].

A semiconductor laser under dc bias can have output power fluctuations reduced below the standard quantum limit [28]. This has been demonstrated with an optically-injected laser under stable locking [29]. Less well understood are the response characteristics of optically-injected lasers operating outside of the stable locking regime. Many of the proposed applications of the optically-injected laser make use of the fact that tunable periodic or aperiodic oscillations of the output power can be generated. Recently, it was demonstrated that, in the regime of limit-cycle periodic dynamics [the so-called period-one (P1) regime], there are operating points where the P1 oscillation frequency could be made essentially insensitive to temperature and bias current fluctuations of the injected laser [1]. At specific combinations of the bias point of the injected laser and the injecting field's amplitude and offset frequency, the P1 frequency becomes locally insensitive to the offset frequency. Simultaneously, the low-frequency modulation of the slave-laser bias current is no longer upshifted to influence the P1 frequency. This is strictly a change in the nonlinear response; the linear response is largely unchanged. It represents a fundamental shift in small- signal sensitivity of the P1 frequency from being dominated by changes in the frequency offset between master and slave lasers to being dominated by the relative amplitude of the injected optical signal.

The objective of this paper is to provide a detailed analysis of the optical spectra of the optically injected semiconductor

Manuscript received January 15, 2014; revised May 26, 2014; accepted June 16, 2014. Date of publication June 22, 2014; date of current version September 1, 2014. The work of T. B. Simpson and J.-M. Liu was supported in part by the Air Force Research Laboratory through a contract with Optimetrics, Inc. The work of N. G. Usechak and V. Kovanis was supported by the Air Force Office of Scientific Research under Grant 12RY09COR. The views and opinions expressed in this paper (88ABW-2013-5365) are those of the authors and do not reflect the official policy or position of the United States Air Force, Department of Defense, or the U.S. Government.

T. B. Simpson is with L-3 Applied Technologies, Inc., San Diego, CA 92121 USA (e-mail: thomas.simpson@l-3com.com).

J.-M. Liu and M. AlMulla are with the Department of Electrical Engineering, University of California Los Angeles, Los Angeles CA 90095USA (e-mail: liu@ee.ucla.edu; almulla@ucla.edu).

N. G. Usechak and V. Kovanis are with the Air Force Research Laboratory, Wright–Patterson AFB OH 45433 USA (e-mail: nicholas.usechak@us.af.mil; vassilios.kovanis@gmail.com).

Color versions of one or more of the figures in this paper are available online at http://ieeexplore.ieee.org.

Digital Object Identifier 10.1109/JLT.2014.2332415

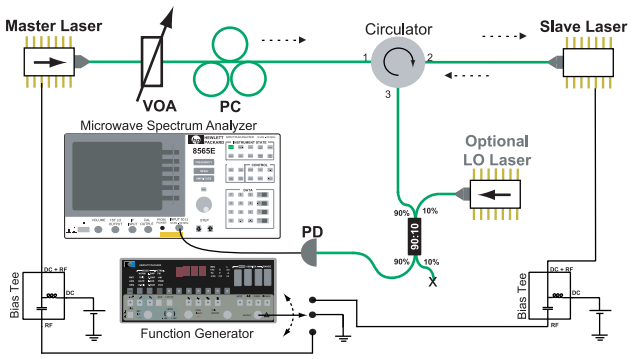

Fig. 1. Schematic of the experimental apparatus. VOA, variable optical attenuator; PC, polarization controller; PD, photodiode. As depicted in the figure, the master and LO lasers were packaged with optical isolators while the slave laser had no isolator. The figure also identifies the propagation direction of the light within the setup using dashed arrows.

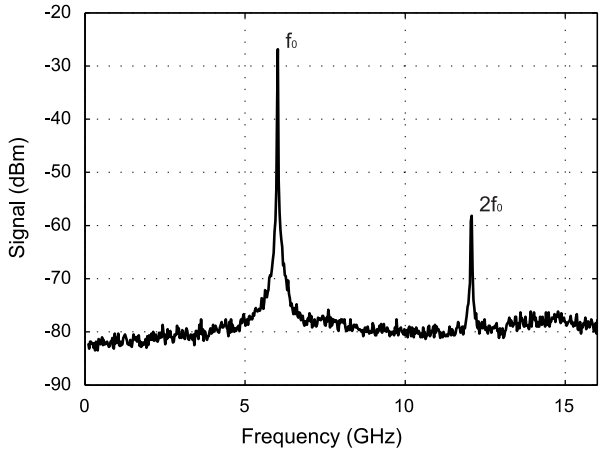

Fig. 2. Power spectrum of the amplified photodiode signal monitoring the output of the optically-injected laser operating in the regime where its output power oscillates at the fundamental resonance frequency. The spectrum displays a strong frequency component at this frequency, f_0, and a weaker one at its second harmonic, $2f_0$. In this case the normalized injection current was $\tilde{J} \approx 1.0$, the normalized injection strength, $\xi \approx 0.02$, and the detuning of the master laser was ≈ -0.3 GHz.

laser undergoing P1 oscillations. The optical spectra consist of a discrete set of strong spectral components and, it is the complex summation of the mixing of these spectral components that yields the optical power spectrum. We emphasize this to show that at certain operating points, this wave mixing of the multiple optical frequency components leads to interference and a cancellation of the response of the P1 oscillation in the power spectrum to low-frequency perturbations. Moreover, we quantify where this occurs in comparison to key bifurcations in the dynamics of the laser system and follow the changes of the P1 frequency at these operating points.

This paper is organized as follows: Section II describes the experimental configuration used to observe and characterize the optical field and power spectra of the injected laser. Section III provides a review of the lumped-element coupled-equation model of the optically injected semiconductor laser. Section IV compares the experimental results to those obtained from the model, focusing on the characteristics of the optical spectra and the behavior of the fundamental (P1) resonance frequency of the system. In this section excellent quantitative agreement between this model (whose parameters have been rigorously determined for this laser [26]) and the experimental data are obtained. We conclude the paper, in Section V, by discussing the implications of these results as they pertain to applications for these devices.

II. Experimental Apparatus and Technique

The experimental apparatus, shown schematically in Fig. 1, is similar to that previously used to map the dynamics of a distributed feedback (DFB) semiconductor laser housed in a butterfly package containing an integrated thermoelectric cooler and pigtailed to a single-mode fiber but lacking an optical isolator [26]. By using the same slave laser in this paper we immediately benefit from the experience obtained through previous studies including apriori knowledge of the laser's parameters. In this paper the slave laser is operated at three times its threshold current where it emits at a wavelength of $\sim$1557 nm. Light is injected into this laser from a second (master) DFB laser, this master laser is packaged with an optical isolator which suppresses the same external feedback effects under study in the slave laser. A fiber-based variable attenuator and an optical circulator are placed between the master and slave lasers, the former to allow control of the injected optical intensity and the latter to increase the optical isolation of the master laser to >60 dB. A fiber-based polarization controller is also used to align the polarization of the master laser to that of the slave. Both lasers are temperature controlled, allowing temperature tuning of the optical frequency, and both are biased using precision current sources. As depicted in the figure, weak radio- and microwave-frequency modulation currents can be added to the bias of either the master or slave laser through bias Tees. For the experiments reported here, the modulation is always weak ($\sim$0.5% peak amplitude) relative to the dc bias, and is fixed at a frequency of 500 MHz. The output of the slave laser is detected by a high-speed photodiode whose output is subsequently amplified and then monitored by an electronic spectrum analyzer (ESA). With just the slave laser output, the power spectrum of the laser output is generated. Alternatively, the slave laser output can be combined in a fiber coupler with the output from a third, temperature-tunable DFB laser that acts as a local oscillator (LO). In this heterodyne case, the electrical spectrum of the photodiode's output serves as a high-resolution measurement of the amplitude spectrum of the optical field. Use of the heterodyne spectrum yields a much higher resolution, limited by the $\sim$1 MHz linewidth of the LO laser, than can be achieved using either a conventional optical spectrum analyzer or a high-finesse Fabry–Perot cavity.

Under optical injection, the slave laser output can become destabilized, which can in turn result in power oscillations. Fig. 2 shows an example of the power spectrum generated by the laser under optical injection in the P1 oscillation regime. It is dominated by a strong peak at the fundamental resonance frequency ($f_0, \sim$6 GHz) and weaker peaks at the harmonics of this frequency. When the laser generates an output with periodic power

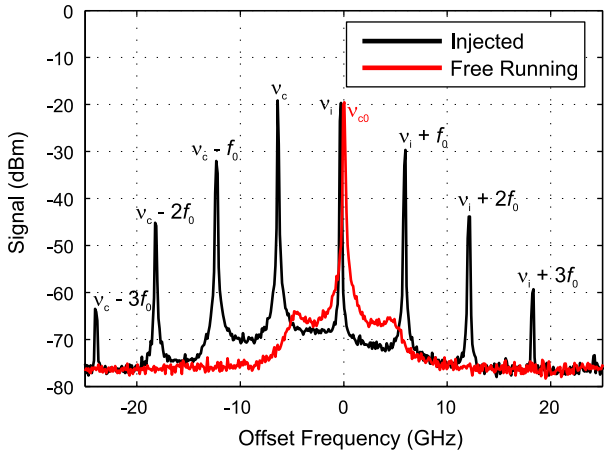

Fig. 3. Heterodyne measurement of the optical frequency spectra generated by sweeping the LO laser frequency across the injected laser output spectrum by ramping the operating temperature. The offset frequency is with respect to the free-running laser output frequency, $\nu_{\rm co}$. Peaks are labeled by their optical frequency. Shown are the spectrum of the free-running laser (red) with its weak, but broad, relaxation resonance frequency sidebands, and the spectrum of the optically injected semiconductor laser operating in the region of power oscillations at the fundamental resonance frequency. In the latter case, the optical injection frequency, $\nu_{\rm i}$, was at the frequency corresponding to the peak just below the optical frequency of the free-running laser, and the pushed laser cavity resonance frequency is $\nu_{\rm c} = \nu_{\rm i} - f_0$. The operating conditions here are the same as in Fig. 2.

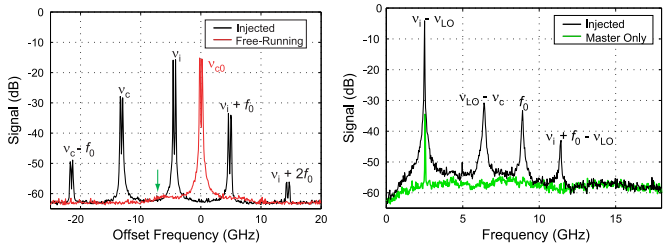

Fig. 4. A comparison of two ways of generating the optical frequency spectrum through heterodyne mixing with a local oscillator. The left panel shows two spectra generated by sweeping the LO laser through the spectrum of the optically injected laser as in Fig. 3. The right panel shows two spectra generated when the LO laser frequency, $\nu_{\rm LO}$, is fixed at the optical frequency indicated by the green arrow in the left panel. The green trace shows the spectrum generated when the slave laser bias current is turned off, showing the beat signal generated by the mixing of the LO laser with the residual master laser output that is scattered off of the front facet of the slave laser and gives the relative frequency of the master laser. The black trace shows the dominant peaks of the combined power and heterodyne spectrum, with the optical spectrum peaks positioned at their relative offsets with respect to the LO laser frequency. For the injected laser there is a strong peak at the injection frequency ($\nu_{\rm i}$), at the injection-shifted laser cavity oscillation frequency ($\nu_{\rm c}$) that is offset by the P1 frequency determined by the strong peak in the power spectrum (f_0), and weaker peaks offset by further P1 frequency shifts. The free-running laser spectrum peak at $\nu_{\rm c0}$ is shown in the left panel but not the right panel. Here the master-laser offset was -4.5 GHz, a normalized injection strength of $\xi = 0.06$ was used, and the slave laser was biased three-times above its threshold current.

oscillations under optical injection, it emits at a discrete set of optical frequencies separated by the characteristic resonance frequency. Fig. 3 shows the optical spectrum of the injected laser in comparison to that of the free-running laser. The spectra are generated by fixing the measurement frequency of the ESA and slowly ramping the temperature, and thus the wavelength, of the LO laser. When the beat frequency of the LO and one of the field components of the slave laser matches the fixed frequency of the ESA, a strong signal is detected. Typically, there are 2 to 4 dominant frequency peaks of the slave laser when operated in the P1 oscillation regime with the two strongest spectral components at the injection frequency, $\nu_{\rm i}$, and at the injection-shifted laser-cavity resonance frequency, $\nu_{\rm c} = \nu_{\rm i} - f_0$. For clarification purposes we point out that, to improve readability, this paper uses ν to define optical frequencies whereas f is used to define microwave frequencies. The free-running laser has a single dominant peak at the laser cavity resonance frequency, $\nu_{\rm c0}$, and weak broad sidebands peaking at approximately the relaxation resonance frequency. The ESA is set to a value of 50 MHz to generate the spectra of Fig. 3. This yields relatively low-resolution optical spectra, due to the double-valued nature of the beat frequency (either positive or negative offset generates a signal). Although they obscure detailed characteristics of the optical frequency components, such as changes due to radio-frequency current modulations, these spectra are very useful for mapping out the dynamic operating characteristics of the laser.

To achieve higher resolutions, the optical frequency of the LO laser can be fixed. In this study, we are specifically interested in the characteristics of the optically injected laser when its output is undergoing periodic power oscillations with a tunable period-one (P1) resonance frequency. In this case the strong spectral components of the P1 oscillation are separated by several gigahertz; therefore, the LO laser can be tuned to an optical frequency between the spectral peaks. Here, the spectrum of the photodiode output consists of the combined power spectrum of the slave laser mixing with itself and the heterodyne spectrum of the mixing of the two lasers. Because the LO laser output is essentially monochromatic, its power spectrum has no spectral features that contribute to our optical spectrum or degrade our results. An example demonstrating this claim is shown in Fig. 4. In this figure the left panel displays the spectra generated by tuning the LO laser (as done in Fig. 3) and identifies the frequency where the LO laser was fixed to generate the spectra shown in the right panel. While care must be taken in the positioning of the LO frequency, it is possible to interpret the spectra to identify the optical frequency components at positive and negative offsets with respect to the LO and the power spectrum peak at the P1 frequency. The spectral position of the peak at the master laser frequency, $\nu_{\rm i}$, is identified by turning off the slave laser and using the small reflected signal of the master laser off the slave laser facet as shown in the figure. Similarly, the spectral position of the free-running laser, $\nu_{\rm c0}$, is established by turning off the master laser, and the position of the P1 peak, f_0, in the power spectrum is established by turning off the LO laser. With this technique the resolution is limited by the 1-MHz linewidth of our LO, provided the spectral features do not overlap. Each of the prominent optical features of the slave laser can be distinguished by properly positioning the output frequency of the LO between the emission peaks of the slave. In our laboratory setup both the master and LO lasers are of the same commercial type and display a nearly

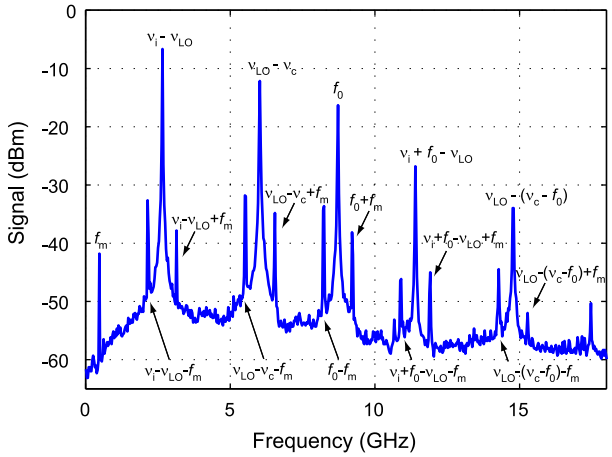

Fig. 5. A spectrum similar to the right panel of Fig. 4 but now showing the modifications due to adding a weak current modulation at 500 MHz to the bias of the optically injected laser. Peaks labeled $f_{\rm m}$ and f_0, and their associated lower and upper sidebands, are the peaks at the modulation and P1 frequency, respectively, in the power spectrum. Peaks labeled with $\nu_{\rm i}$, $\nu_{\rm c}$, $\nu_{\rm i}+f_0$, and $\nu_{\rm i}-f_0$, with associated sidebands, are from the optical spectrum. See text for further identification of all of the peaks in the heterodyne spectrum. The frequency axis is as measured by the ESA and so the positions of the heterodyne peaks from the optical spectrum depend on the offset with respect to the local oscillator laser frequency, $\nu_{\rm LO}$. Here the master-laser offset was -3.1 GHz, a normalized injection strength of $\xi = 0.06$ was used, and the slave laser was biased three-times above its threshold current.

identical tuning characteristic with temperature of -11.5 GHz/C, which makes it relatively straightforward to keep the LO laser frequency properly positioned relative to the slave laser output spectrum as the master laser's optical frequency is tuned.

In this paper, we add a weak modulation current to the dc bias of either the master or slave laser in order to investigate the resulting spectral properties. This modulation adds negatively and positively offset sidebands to each of the strong optical-field components, as shown in Fig. 5 , where all of the labeled peaks can be identified. From the power spectrum there are peaks at the 500-MHz modulation frequency (labeled $f_{\rm m}$) and at the P1 frequency and its upper and lower sidebands, labeled f_0, $f_0+f_{\rm m}$, and $f_0-f_{\rm m}$ respectively. Additionally, the heterodyne spectrum adds peaks due to mixing between the LO ($\nu_{\rm LO}$) and the components and sidebands that are associated with the master laser injection frequency ($\nu_{\rm i}$, $\nu_{\rm i}+f_{\rm m}$, and $\nu_{\rm i}-f_{\rm m}$), the injection-shifted, slave-laser cavity resonance frequency ($\nu_{\rm c}$, $\nu_{\rm c}+f_{\rm m}$, and $\nu_{\rm c}-f_{\rm m}$), the component one P1 frequency offset above the master laser ($\nu_{\rm i}+f_0$), and the component one P1 frequency offset below the pushed frequency peak ($\nu_{\rm c}-f_0$). (Note that the data in the right panel of Fig. 4 and in Fig. 5 are the raw data from the ESA. The values taken from such spectra and used in subsequent figures have been corrected for the response characteristics of the measurement system.) The amplitudes of all of the sidebands vary in nontrivial ways as a control parameter such as the frequency detuning between the master laser and the free-running slave laser is varied. The sidebands of each optical field component mix with the adjacent central feature of the adjacent field components to produce the sidebands on either side of the P1 frequency feature in the power spectrum. This complex summation and mixing can lead to destructive interference, a feature that can be recovered in the standard lumped-element coupled-equation model of the injected laser system that we review next.

III. Theoretical Model

The output from a laser subject to an externally injected field can be described by a set of coupled equations relating the circulating optical field, the polarization and the population density of the gain medium, and the injected optical signals [30]. Specifically, for the case of a semiconductor laser subject to near-resonant external optical injection the coupled equations for the circulating optical field, $A(t)e^{-i\omega_{\rm c0}t}$, where $\omega_{\rm c0}$ is the optical frequency of the free-running laser, and the carrier density of the gain medium, $N(t)$ simplify to [26]

$$\frac{dA}{dt} = \left[-\frac{\gamma_{\rm c}}{2} + i(\omega_{\rm c0}-\omega_{\rm cc})\right]A + \frac{\Gamma}{2}g(N,|A|)A + \eta A_{\rm i}e^{-i(\omega_{\rm i}-\omega_{\rm c0})t} \tag{1}$$

$$\frac{dN}{dt} = \frac{J}{ed} - \gamma_{\rm s}N - \frac{2\epsilon_0 n^2}{\hbar\omega_{\rm c0}}\bar{g}(N,|A|)|A|^2 \tag{2}$$

$$\bar{g}(N,|A|) \stackrel{def}{=} Re\left[g(N,|A|)\right] \tag{3}$$

$$g(N,|A|) = g_0(N_0,A_0) + (1-ib)\left.\frac{\partial\bar{g}}{\partial N}\right|_{N_0,A_0}(N-N_0) + (1-ib')\left.\frac{\partial\bar{g}}{\partial|A|^2}\right|_{N_0,A_0}\left(|A|^2-A_0^2\right). \tag{4}$$

Here, the semiconductor laser is modeled as a single-mode lumped element subject to an injected laser beam of constant amplitude, $A_{\rm i}$, and constant optical frequency $\omega_{\rm i}=2\pi\nu_{\rm i}$. The laser cavity is described in terms of $\gamma_{\rm c}$, the cavity decay rate, $\omega_{\rm c0}=2\pi\nu_{\rm c0}$, the free-running cavity oscillation frequency, $\omega_{\rm cc}=2\pi\nu_{\rm cc}$, the cold-cavity (carrier-free) resonance frequency, and Γ, the confinement factor that relates the overlap of the oscillating mode with the gain medium, The injection coupling rate, η, quantifies the coupling of the externally injected laser beam into the slave laser cavity. The carrier density injection rate is J/ed where J is the injected current density (e is the electronic charge and d is the thickness of the gain medium), $\gamma_{\rm s}$ is the carrier spontaneous decay rate, $\epsilon_0 n^2$ is the non-resonant (real) permittivity of the semiconductor gain medium, and $\hbar$ is Plancks constant. When free-running, in other words with no injected laser beam, the laser operates at an optical frequency $\omega_{\rm c0}$ with a steady-state amplitude A_0 and a steady-state carrier density N_0. The complex gain, $g(N,|A|)$, controls the characteristics of the laser cavity and depends on the carrier density and the magnitude of the laser amplitude. The real part of the gain, $\bar{g}(N,|A|)$, describes the transfer of power between the semiconductor gain medium and the laser beam, while the imaginary part describes how the dielectric constant (and through it the laser cavity resonance frequency) changes in the laser. Both parts are assumed to vary about the free-running, steady-state operating point, $g_0(N_0,|A_0|)$, as a linear function of the changes in

the carrier density and the laser intensity (proportional to the square of the laser field magnitude). In (4), b is the ratio of the imaginary to real parts of the complex gain due to carrier density changes, and b' is the ratio due to saturation effects. The latter ratio is not generally used in describing semiconductor lasers, but is essential for the quantitative modeling done here [5], [26]. Just as b was originally introduced to account for the enhanced linewidth of semiconductor lasers, and saturation effects (related to $\frac{\partial \bar{g}}{\partial |A|^2}$) were introduced to account for the low-frequency rolloff in the modulation response, b' was introduced to account for the asymmetry of the optical spectrum in response to a modulation current [5]. It is generally expected to be present in a detuned two-level system [31], [32]. Equation (4) gives the general, first-order expansion of the gain in terms of changes to the carrier density and optical intensity; it does not rely on a specific quantum model of the gain medium. It assumes that the carriers involved in the optical transition come into equilibrium with all carriers on times scales short compared to those of interest for the dynamics. This is expected to be true of most semiconductor laser media and the model has been successfully applied to a wide range of lasers based on different cavity configurations (Fabry–Perot, DFB, VCSEL, etc.) and materials (heterostructure, quantum well, and a variety of III-V alloys). However, recent work on quantum-dot semiconductor lasers, and indeed the whole rationale for their use, indicates that the quantum-confined carriers involved in the optical transition need to be considered separately from the background carriers in the non-localized energy bands [33], [34]. The appropriate lowest-order model for this gain medium is still the subject of debate and ongoing research. More complex laser structures, such as multi-section lasers, could still conceivably be treated as a lumped element but all sections would require appropriate equations for their respective carrier dynamics, and the appropriateness of the single-spatial mode approximation would need to be determined. Finally, we do not include spontaneous emission in the work here because in our experiments the external optical injection and deterministic interactions are strong enough to dominate the dynamics of the problem. The spontaneous emission plays a role in determining the linewidth of the various peaks in the optical spectrum (excepting the peak at the injection frequency), but otherwise acts as a perturbing noise source that sets the noise floor for the spectra.

Equation (1) is the equation for the complex field, A. For numerical modeling it is convenient to introduce $A(t)e^{-i\omega_{c0}t} = A_0 e^{-i\omega_i t}\left[a_1(t) + ia_2(t)\right]$ and $N = N_0\left[1+n\right]$ to generate two real equations for the field components in-phase and in-quadrature with respect to the master laser ([1] and its supplementary material)

$$\frac{da_1}{dt} = -\Omega a_2 + \gamma_c \xi + \frac{\gamma_c}{2}\left[\frac{\gamma_n}{\gamma_s \tilde{J}}\tilde{n}\left(a_1 + b a_2\right) - \frac{\gamma_p}{\gamma_c}\left(a_1^2 + a_2^2 - 1\right)\left(a_1 + b' a_2\right)\right] \tag{5}$$

TABLE I
PARAMETER VALUES USED IN NUMERICAL SIMULATIONS

Term	Description	Value	Units	Error
b	Linewidth Enhance. Factor	3.0	N/A	$+10/-20\%$
b'	Nonlinear Gain Ratio	-1.5	N/A	$\pm 50\%$
γ_c	Cavity Photon Decay Rate	5.4×10^{11}	s^{-1}	$\pm 10\%$
γ_s	Carrier Spont. Decay Rate	4×10^9	s^{-1}	$\pm 10\%$
γ_n	Differential Gain Relax. Rate	$1.7 \times 10^9 \cdot \tilde{J}$	s^{-1}	$\pm 10\%$
γ_p	Nonlinear Gain Relax. Rate	$5.0 \times 10^9 \cdot \tilde{J}$	s^{-1}	$\pm 10\%$

$$\frac{da_2}{dt} = \Omega a_1 + \frac{\gamma_c}{2}\left[\frac{\gamma_n}{\gamma_s \tilde{J}}\tilde{n}\left(-b a_1 + a_2\right) - \frac{\gamma_p}{\gamma_c}\left(a_1^2 + a_2^2 - 1\right)\left(-b' a_1 + a_2\right)\right]. \tag{6}$$

In these equations, $\gamma_n = \frac{2\epsilon_0 n^2}{\hbar \omega_{c0}} \frac{\partial \bar{g}}{\partial N}\Big|_{A_0, N_0} A_0^2$, $\gamma_p = -\Gamma \frac{\partial \bar{g}}{\partial |A|^2}\Big|_{A_0, N_0} A_0^2$, and $\tilde{J} = \left(\frac{J_0}{ed} - \gamma_s N_0\right)/(\gamma_s N_0)$ where J_0 is the steady-state injection current, $\xi = \frac{\eta A_i}{\gamma_c A_0}$, and $\Omega = \omega_i - \omega_{c0}$. The equation for the carrier density can be written as

$$\frac{d\tilde{n}}{dt} = \gamma_s\left(\tilde{J} + 1\right)\frac{J_m}{J_0} - \left[\gamma_s + \gamma_n(a_1^2 + a_2^2)\right]\tilde{n} - \gamma_s \tilde{J}\left[1 - \frac{\gamma_p}{\gamma_c}(a_1^2 + a_2^2)\right]\left(a_1^2 + a_2^2 - 1\right) \tag{7}$$

where J_m is any time-dependent part of the injection current. The laser parameters can be experimentally determined [5], [6] while $\tilde{J}$, $\frac{J_m}{J_0}$, Ω, and ξ can be varied in the experiment. The model calculations use the experimentally determined parameters listed in Table I for the injected laser [1] biased at $\tilde{J} \sim 2.0$. In these experiments $\frac{J_m}{J_0} \ll 1$.

For the free-running laser, the relaxation resonance frequency is given by $\sqrt{\gamma_n \gamma_c + \gamma_s \gamma_p}$ and the associated damping rate by $\gamma_s + \gamma_n + \gamma_p$. Note that because γ_c is approximately two orders of magnitude larger than the other rates, the relaxation resonance frequency is typically much larger than the damping rate and is only weakly dependent on the nonlinear gain relaxation rate. Because of this, one can get good semi-quantitative agreement between model and experiment even with $\gamma_p = 0$, or equivalently $\frac{\partial \bar{g}}{\partial |A|^2} = 0$ [35]. As a consequence, all of the key experimentally measured features of the optically injected semiconductor laser discussed in this paper can be reproduced with $\gamma_p = 0$ (and a modified value of b), but at significantly offset values of the detuning frequency and injection parameter relative to the experimentally measured values.

Numerical simulations of the optically injected semiconductor laser based on (4)–(7) used a Runge–Kutta integration procedure over durations $> 1\mu$s to generate time series that were subsequently Fourier transformed to produce spectra [13] that could be directly compared with the experimentally measured spectra. Fig. 6 shows a calculated mapping of the dynamics regions overlaid with the curves of constant P1 frequency.

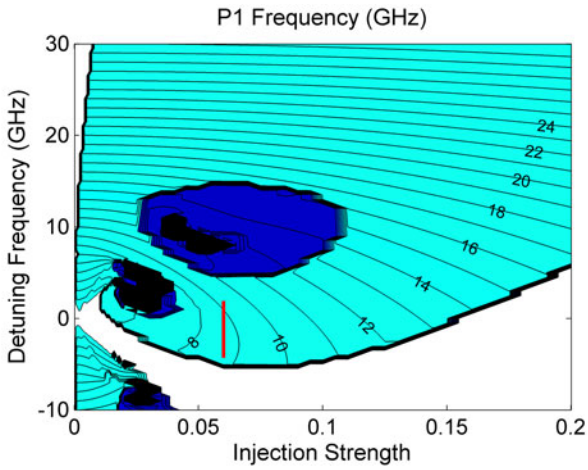

Fig. 6. Mapping of the dynamics of the optically injected semiconductor laser as a function of the strength and offset frequency of the master laser. The white region is stable injection locking, the large multicolored region displays power oscillations at the P1 frequency, with lines of constant oscillation frequency displayed. Dark blue to black are regions of period doubling of the fundamental resonance and more complex dynamics. Also drawn is a vertical line locating the operating conditions for data displayed in subsequent figures.

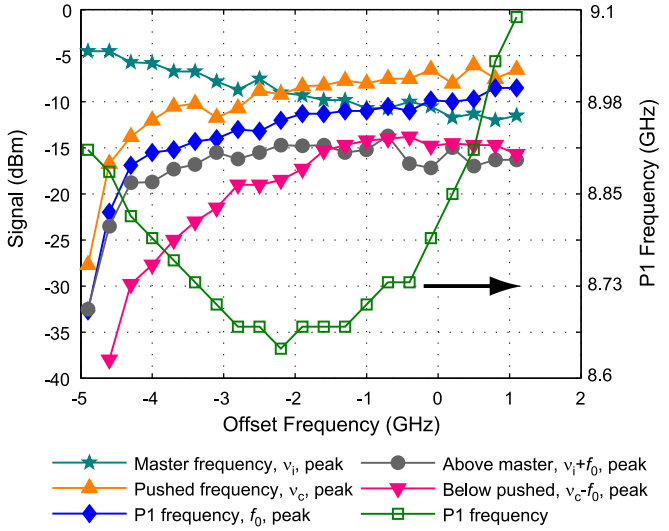

Fig. 7. Experimentally measured amplitudes of the various optical frequency components, and the component in the power spectrum at the P1 resonance frequency, f_0, as the master laser detuning is varied along the vertical line superimposed in Fig. 6. The master frequency peak is at the injection frequency of the master laser, ν_i, the pushed laser cavity peak is offset by the P1 frequency below this value, $\nu_c = \nu_i - f_0$, and the other two are for the peaks above $(\nu_i + f_0)$ and below $(\nu_c - f_0)$ these central peaks. Also shown is the value of the P1 frequency (right axis).

The region of P1 dynamics as a function of the master laser detuning frequency is bounded from below by a Hopf bifurcation to stable locking, and in certain regions by transitions to more complex periodic (period-doubling and higher) and aperiodic (quasiperiodic and chaotic) dynamics. This mapping is in quantitative agreement with the experimentally observed dynamical characteristics of the laser. Note that there is a line of operating points extending from near the minimum offset of the Hopf bifurcation to the upper edge of lower amplitude and offset region of complex dynamics where the P1 frequency becomes locally insensitive to changes in the offset frequency between master and slave lasers. We will emphasize these operating points below, specifically detailing how the optical spectra change as the master laser detuning is varied in the regions around these operating points.

IV. Results: Experimental Measurements and Numerical Simulations

As one moves around the map of Fig. 6, by changing the injected amplitude (varying the master laser bias current or the attenuation between the master and slave lasers) or offset frequency (varying the operating temperature of the master laser), changes in the optical heterodyne spectra and the power spectra are observed, even within the region of P1 dynamics. For instance, as one moves along the line in Fig. 6 away from the Hopf bifurcation separating the P1 dynamics region from the region of stable locking, the strong peaks in the optical spectra and the power spectra change in amplitude and frequency as shown in Fig. 7. The optical peak at the injection frequency decreases in amplitude, while the other optical peaks first grow stronger, then level off and finally begin to decrease in amplitude. The P1 frequency first decreases, passes through a minimum and then increases. Note that the offset for the P1 minimum is close to

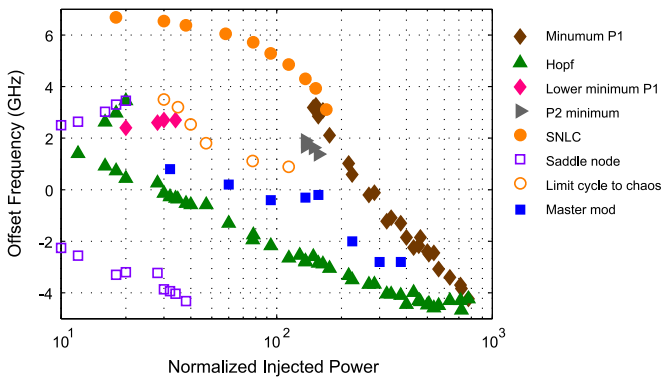

Fig. 8. Mapping of key operating points experimentally measured in this investigation. See text for details. SNLC = saddle node of limit cycle bifurcation, Master Mod = minimum sensitivity for modulation current added to the master laser. The slave laser modulation minima overlap with the P1 minima that run from the SNLC bifurcation to the Hopf bifurcation. The normalized injection power (= 10.0) is at the same injection strength as $\xi = 0.01$.

the offset where the two dominant optical peaks, at the injection frequency and at the pushed cavity resonance frequency that is offset by the P1 frequency, are of the same amplitude.

Operating points where the P1 frequency is at an extremum with respect to changes in a control parameter are of particular interest because they show local insensitivity to perturbations in that parameter. Because of the application potential for these regions, we set out to find such extrema and better understand them. These results are summarized in Fig. 8 which shows a mapping of local sensitivity minima with respect to some variation along with key bifurcations as the detuning between master and slave laser is varied. Starting from negative offsets

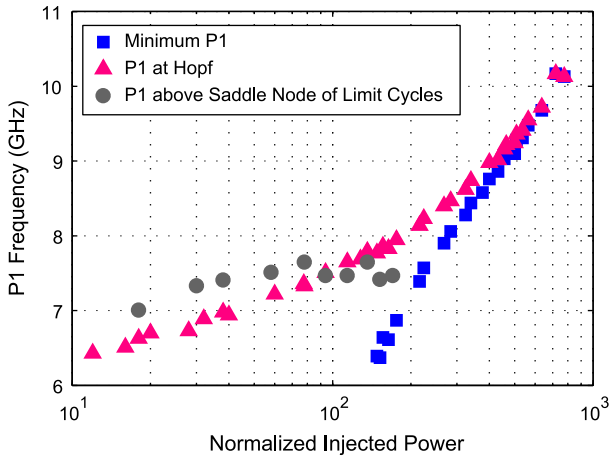

Fig. 9. The P1 resonance frequency just above the Hopf and saddle-node of limit cycle bifurcations shown in Fig. 8, and at the operating points where the P1 frequency and the sensitivity to current fluctuations are simultaneously minimized. The saddle-node of limit cycles bifurcation ends when the minimum P1 frequency intersects. The normalized injection power (=10.0) is at the same injection strength as $\xi = 0.01$.

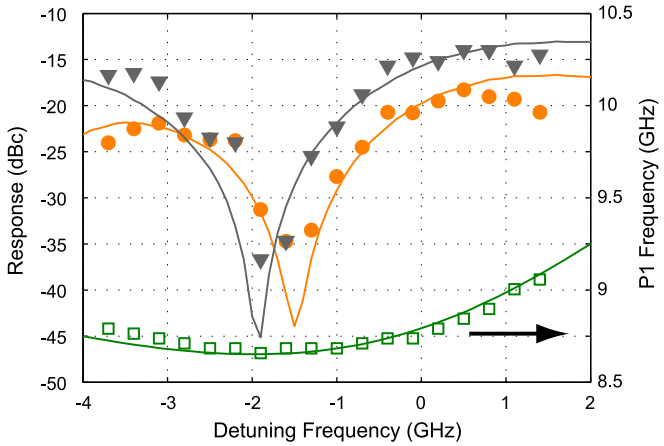

Fig. 10. Experimentally measured (symbols) and calculated (solid curves) values of the modulation sideband amplitude and the P1 frequency using a normalized injection amplitude of $\xi = 0.06$ when the current modulation is applied to the slave laser. This figure shows the positive frequency detuning sideband (solid circles, corresponding to peak $f_0 + f_m$ in Fig. 5), the negative detuning sideband (solid triangles, corresponding to peak $f_0 - f_m$ in Fig. 5), and the corresponding P1 frequency (open squares, corresponding to the frequency of the peak labeled f_0 in Fig. 5).

and working up, the region of stable locking is bounded by saddle-node (open squares; purple) and Hopf (sold triangles; green) bifurcations. Above the Hopf bifurcation is the region of limit-cycle oscillations at the P1 frequency. There is a bounded range of chaotic dynamics that from below shows period-doubling routes to chaos (open circles; orange), and from above shows an abrupt saddle-node of limit cycle (SNLC) bifurcation (solid circles; orange) [25]. On either side of the region of chaotic dynamics there are local minima in the P1 frequency. At low injection levels a range (solid diamonds; pink) runs down to near the upper frequency bound on the Hopf bifurcation. On the high injection side of the chaotic dynamics region there are two ranges, a short one associated with a period-doubling route from/to chaos (solid right-facing triangles; gray) and a more extensive one that runs between the SNLCs bifurcation and the Hopf bifurcation (solid diamonds; brown). Fig. 9 shows how the frequencies of the P1 minima compare with those along the Hopf and SNLC bifurcations as a function of the injection strength. In Fig. 9, the SNLCs terminates when its frequency matches the P1 minimum frequency at the same optical injection level [36]. If the laser bias is changed, the P1 minima can terminate in the region of complex dynamics close to this bifurcation. In addition to minima in the P1 frequency with respect to detuning, we searched for minima in the sensitivity of the P1 frequency to modulation of the bias current to either the master or slave laser. For modulation of the slave laser current, we observed that the sensitivity was also minimized along the curve of brown diamonds in Fig. 8, coincident with the P1 minimum with respect to detuning. Fig. 10 shows the dramatic decrease in response of the sidebands around the P1 frequency peak as the master-slave frequency offset is varied along the line denoted in Fig. 6. For modulations to the master laser current, there is a separate range denoted by the solid blue squares (Master Mod) in Fig. 8 that are offset from the P1 frequency minima. These minima are offset because changes to the master laser current change the amplitude of the injected optical signal to the slave laser directly modifying the circulating optical field, a different perturbation to the laser system than a current modulation to the interaction gain medium that directly modifies the carrier density.

A close inspection of Fig. 10 shows that the minima of the two sidebands are offset with respect to each other and to the P1 frequency minimum with respect to detuning. This is clearest in the numerical data, which is not corrupted by noise or other experimental artifacts. The offset with respect to each other is a monotonically increasing function with respect to the modulation frequency. Calculations show that the offset with respect to the P1 frequency minimum is a complex function of the various dynamic parameters, in particular the parameter b' [31].

The set of operating points where there is the simultaneous minimum of the P1 frequency with respect to detuning and sensitivity minimum to current modulation of the slave laser is of particular interest due to the fact that it represents operation where sensitivity to current and temperature fluctuations of the slave laser are minimized, and simultaneously where sensitivity to temperature (but not current) fluctuations of the master are minimized. Therefore, we investigated the changes to the optical spectra along the detuning line of Fig. 6 in greater detail in Fig. 11. Here, the sideband signal amplitude, normalized to the amplitude of its associated center peak, is shown as the master laser detuning frequency is varied. The sidebands of each of the four strongest peaks in the optical spectrum display different characteristics as the detuning is changed. In no case is the minimum among the sidebands of the various optical peaks as deep as the sensitivity minimum of the sidebands in the power spectrum. Moreover, the linear modulation peak, the peak in the power spectrum at the modulation frequency, shows no dip unlike any of the optical spectrum sidebands. This is compelling evidence that the minimization in sensitivity in the

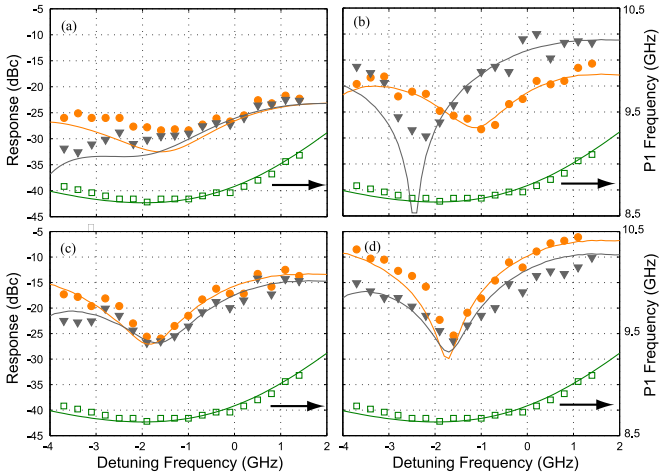

Fig. 11. Experimentally measured (solid symbols) and calculated (solid curves) values of the modulation sideband amplitudes of a normalized injection amplitude of $\xi = 0.06$. This figure shows the positive frequency detuning sideband ($+f_{\rm m}$, solid circles), the negative detuning sideband ($-f_{\rm m}$, solid triangles), and the corresponding P1 frequency (open squares). Upper left is for the optical frequency component at the frequency of the injected optical signal (corresponding to peak $\nu_{\rm i}$ in Fig. 5). Lower left is for the component at the pushed laser cavity resonance frequency (corresponding to peak $\nu_{\rm c}$ in Fig. 5), one P1 frequency below the injection frequency. Upper right is for the sideband one P1 frequency above the injection frequency (corresponding to peak $\nu_{\rm i} + f_0$ in Fig. 5), and lower right is twice the P1 frequency below the injection frequency (corresponding to peak $\nu_{\rm c} - f_0$ in Fig. 5).

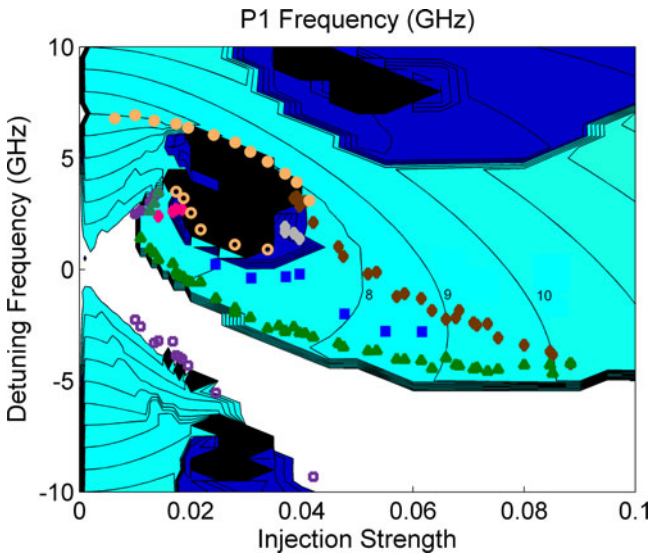

Fig. 12. Mapping combining the calculated values of Fig. 6 and the experimentally measured values of Fig. 8.

power spectrum, displayed in Fig. 10, arises from a complex summation involving wave mixing in all of the optical peaks.

V. Discussion and Conclusions

Combining the numerical mapping results of Fig. 5 and the experimental measurements of Fig. 8 yields the comparison map of Fig. 12 that shows the accuracy of the lumped-element model in describing the experimental results. Because it is extremely difficult to determine the actual power injected into the slave laser through the fiber-optic coupling path, this is used as our only fitting parameter. Nevertheless, it is determined by fitting the negative offset saddle-node bifurcation experimental data to the model predictions. This then fully determines the experimental map and the agreement is excellent. Further, the agreement between data and model in Fig. 11 shows that even detailed features of the system can be fully recovered in quantitative agreement. This degree of accuracy requires careful determination of the dynamic parameters that go into the model. The parameters relating the real (gain) and imaginary (refractive index) parts of the complex gain to changes in the carrier density and circulating intensity are particularly important for setting the positions of the Hopf and saddle-node bifurcations, which strongly depend on the linewidth enhancement factor, b [37]. The gain saturation factor, b', plays a critical role in determining the offsets of the various minima in sensitivity [31]. The various relaxation rates determine the magnitude of the P1 frequency [38]. Recent numerical calculations show that all of these terms play a role in determining the positions of the sensitivity minima within the overall mapping as a function of injection amplitude and frequency offset [31]. Numerical work also suggests that allowable values of b for the observation of the sensitivity minima are bounded both from below and above. Saturation effects do not have to be included for the observation of sensitivity minima. Therefore, they are not determined by nonlinear gain effects such as spectral hole burning or carrier heating. It is the interband carrier dynamics, and their effects on the refractive index of the gain medium, that principally determine when the wave mixing of the various optical frequency components will lead to destructive interference and the minimization of sensitivity to perturbations. Saturation effects, and nonlinear gain effects in general, do play a key role in the relative positioning of the sensitivity minima with respect to the various bifurcations in the mapping.

Because of the excellent agreement between experimental data and numerical results, we have confidence that the numerical simulations give an accurate representation of system dynamics, including features that are not easily accessible by experiment. Specifically, the numerical simulations can be used to investigate the modulation characteristics of the carrier density. Fig. 13 compares the calculated amplitude of the sidebands of the P1 frequency peak in the power spectrum with the same sidebands in the carrier spectrum. The latter have been offset by $+17$ dB for the negative sideband and by $+18$ dB for the positive one from their calculated values to show the strong similarity between the changes in the sideband amplitudes in the two spectra as the offset frequency of the master laser is varied. The interference among the various optical frequency components that minimizes the amplitude of the power spectrum sidebands simultaneously drives down the sensitivity of the carrier density around these special operating points. There is minimal response of the medium to the nonlinear interaction of the optical frequency components for frequencies near the P1 resonance frequency, while the linear response to the induced current modulation is essentially unchanged. Modulating the master laser bias current simultaneously changes the

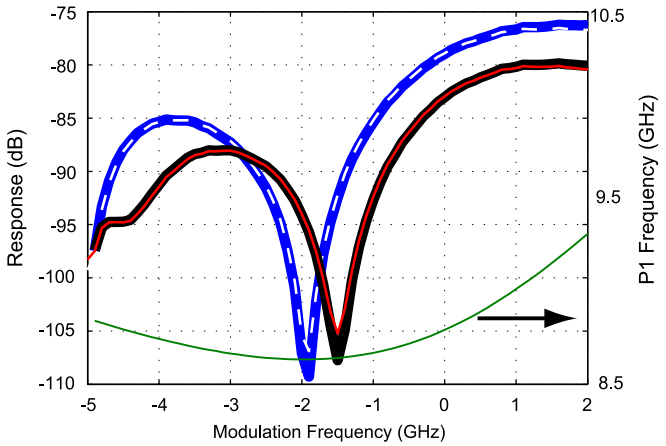

Fig. 13. Calculated values of the P1 peak sideband amplitudes as a function of master laser detuning for the intensity and carrier spectra: (solid black) intensity upper sideband, (solid blue) intensity lower sideband, (solid red) carrier upper, and (dashed white) carrier lower. The carrier lower sideband has been offset by +17 dB and the carrier upper sideband by +18 dB to emphasize the similarity with the corresponding intensity sideband. Also shown is the P1 frequency (solid green).

amplitude and frequency of the detuning so that the operating point would move along a diagonal line in Fig. 12, not a vertical line as is the case for temperature fluctuations. Because the injected amplitude is changing, this perturbation directly influences the optical field in (5) through a modulated injection term, ξ, rather than through the carrier density in (7) as is the case when the slave laser bias current is modulated. Past work has demonstrated AM-to-FM conversion in the P1 dynamics of the optically injected semiconductor laser [14]. The slave laser modulation current primarily induces a frequency modulation and so its influence on the P1 frequency is suppressed at these operating points. However, the laser remains sensitive to fluctuations in the amplitude of the injected signal.

These results are interesting on two levels. On a basic level, the quantitative agreement between theory and modeling allows new tests of semiconductor laser characteristics and dynamic parameters based on the interactions described here. For instance, there is considerable current interest in the dynamics of quantum-dot lasers and the precision of the techniques described here will allow rigorous testing of proposed modifications to the coupled equation model to characterize these novel structures. Further the observed ability to reduce the sensitivity of semiconductor laser limit-cycle dynamics to system perturbations has received very little attention to date, and the general characteristics are not well understood. Past work has established that the amplitude stability of free-running and stably-locked semiconductor lasers can be increased beyond the standard quantum limit [28], [29]. Here in contrast we have demonstrated that the fundamental resonance frequency in the optically injected laser can be made insensitive to fluctuations in the laser current and operating temperature so that it is only sensitive to the amplitude of the injected optical signal from the master laser. This leads to the second interesting aspect of this paper: Photonic oscillators have been proposed for a variety of applications and the discovery of these operating points shows that the optically injected laser may be able to display favorable phase noise and jitter characteristics to go along with its wide tuning range [21], [24]. Potentially, these operating points can be complemented by other nonlinear dynamics noise reduction techniques such as those recently implemented in nanomechanical oscillators [39]. Now additional work is needed to see if these observations can be translated into improved performance of photonic devices such as broadly tunable, low-noise, low-jitter oscillators.

REFERENCES

[1] T. B. Simpson, J.-M. Liu, M. AlMulla, N. G. Usechak, and V. Kovanis, "Novel limit-cycle dynamics with reduced sensitivity to perturbations," *Phys. Rev. Lett.*, vol. 112, p. 023901, 2014.

[2] G. P. Agrawal, and N. K. Dutta, *Long Wavelength Semiconductor Lasers*, 1st ed. New York, NY, USA: Academic, 1986.

[3] T. Erneux, and P. Glorieux, *Laser Dynamics*, 1st ed. London, U.K.: Cambridge Univ. Press, 2010.

[4] J.-M. Liu and T. B. Simpson, "Characterization of fundamental parameters of a semiconductor laser with an injected optical probe," *IEEE Photon. Technol. Lett.*, vol. 5, no. 4, pp. 380–382, Apr. 1993.

[5] T. B. Simpson, F. Doft, E. Strzelecka, J.-M. Liu, W. Chang, and G. J. Simonis, "Gain saturation and the linewidth enhancement factor in semiconductor lasers," *IEEE Photon. Technol. Lett.*, vol. 13, no. 8, pp. 776–778, Aug. 2001.

[6] G. Liu, X. Jin, and S.-L. Chuang, "Measurement of linewidth enhancement factor of semiconductor lasers using an injection-locking technique," *IEEE Photon. Technol. Lett.*, vol. 13, no. 5, pp. 430–432, May 2001.

[7] K. E. Chlouverakis, K. M. Al-Aswad, I. D. Henning, and M. J. Adams, "Determining laser linewidth parameter from HOPF bifurcation minimum in lasers subject to optical injection," *IEE Electron. Lett.*, vol. 39, pp. 1185–1187, 2003.

[8] N. M. Al-Hosiny, I. D. Henning, and M. J. Adams, "Correlation of electron density changes with optical frequency shifts in optically injected semiconductor lasers," *IEEE J. Quantum Electron.*, vol. 42, no. 6, pp. 570–580, Jun. 2006.

[9] T. B. Simpson, J.-M. Liu, and A. Gavrielides, "Bandwidth enhancement and broadband noise reduction in injection-locked semiconductor lasers," *IEEE Photon. Technol. Lett.*, vol. 7, no. 7, pp. 709–711, Jul. 1995.

[10] J. Wang, M. K. Haldar, L. Li, and F. Mendis, "Enhancement of modulation bandwidth of laser diodes by injection locking," *IEEE Photon. Technol. Lett.*, vol. 8, no. 1, pp. 34–36, Jan. 1996.

[11] G. Yabre, "Effect of relatively strong light injection on the chirp-to-power ratio and the 3 db bandwidth of directly modulated semiconductor lasers," *J. Lightw. Technol.*, vol. 14, no. 10, pp. 2367–2373, Oct. 1996.

[12] X. J. Meng, T. Chau, and M. C. Wu, "Experimental demonstration of modulation bandwidth enhancement in distributed feedback lasers with external light injection," *IEE Electron. Lett.*, vol. 34, pp. 2031–2032, 1998.

[13] S. C. Chan, S. K. Hwang, and J.-M. Liu, "Period-one oscillation for photonic microwave transmission using an optically injected semiconductor laser," *Opt. Exp.*, vol. 15, pp. 14921–14935, 2007.

[14] S. C. Chan, S. K. Hwang, and J. M. Liu, "Radio-over-fiber AM-to-FM upconversion using an optically injected semiconductor laser," *Opt. Lett.*, vol. 31, pp. 2254–2256, 2006.

[15] S.-K. Hwang, H.-F. Chen, and C.-Y. Lin, "All-optical frequency conversion using nonlinear dynamics of semiconductor lasers," *Opt. Lett.*, vol. 34, pp. 812–814, 2009.

[16] C. H. Chu, S. L. Lin, S. C. Chan, and S. K. Hwang, "All-optical modulation format conversion using nonlinear dynamics of semiconductor lasers," *IEEE J. Quantum Electron.*, vol. 48, no. 11, pp. 1389–1396, Nov. 2012.

[17] F. Y. Lin and J.-M. Liu, "Chaotic radar using nonlinear laser dynamics," *IEEE J. Quantum Electron.*, vol. 40, no. 6, pp. 815–820, Jun. 2004.

[18] F. Y. Lin, and J. M. Liu, "Chaotic Lidar using nonlinear laser dynamics," *IEEE J. Sel. Topics Quantum Electron.*, vol. 10, no. 5, pp. 991–997, Sep./Oct. 2004.

[19] J.-M. Liu, H. F. Chen, and S. Tang, "Optical-communication systems based on chaos in semiconductor lasers," *IEEE Trans. Circuits Syst. I, Fundam. Theory Appl.*, vol. 48, no. 12, pp. 1475–1483, Dec. 2001.

[20] K. Hirano, T. Yamazaki, S. Morikatsu, H. Okumura, H. Aida, A. Uchida, S. Yoshimori, K. Yoshimura, T. Harayama, and P. Davis, "Fast random

bit generation with bandwidth-enhanced chaos in semiconductor lasers," *Opt. Exp.*, vol. 18, pp. 5512–5524, 2010.

[21] S. Chan and J.-M. Liu, "Tunable narrow-linewidth photonic microwave generation using semiconductor laser dynamics," *IEEE J. Sel. Topics Quantum Electron.*, vol. 10, no. 5, pp. 1025–1032, Sep.–Oct. 2004.

[22] S. Hyuk-Kee, Z. Xiaoxue, E. K. Lau, D. Parekh, C. Chang-Hasnain, and M. C. Wu, "Optoelectronic oscillators using direct-modulated semiconductor lasers under strong optical injection," *IEEE J. Sel. Topics Quantum Electron.*, vol. 15, no. 3, pp. 572–577, May–Jun. 2009.

[23] T. B. Simpson, J.-M. Liu, M. AlMulla, N. G. Usechak, and V. Kovanis, "Linewidth sharpening via polarization-rotated feedback in optically-injected semiconductor laser oscillators," *IEEE J. Sel. Topics Quantum Electron.*, vol. 19, pp. 1500807-1–1500807-7, Jul./Aug. 2013.

[24] J. P. Zhuang and S. C. Chan, "Tunable photonic microwave generation using optically injected semiconductor laser dynamics with optical feedback stabilization," *Opt. Lett.*, vol. 38, pp. 344–346, 2013.

[25] S. Wieczorek, B. Krauskopf, T. B. Simpson, and D. Lenstra, "The dynamical complexity of optically injected semiconductor lasers," *Phys. Rep.*, vol. 416, pp. 1–128, 2005.

[26] T. B. Simpson, "Mapping the nonlinear dynamics of a distributed feedback semiconductor laser subject to external optical injection," *Opt. Commun.*, vol. 215, pp. 135–151, 2003.

[27] T. B. Simpson, J.-M. Liu, A. Gavrielides, V. Kovanis, and P. M. Alsing, "Period-doubling cascades and chaos in a semiconductor laser with optical injection," *Phys. Rev. A*, vol. 51, pp. 4181–4185, 1995.

[28] Y. Yamamoto, S. Machida, and O. Nilsson, "Amplitude squeezing in a pump-noise-suppressed laser oscillator," *Phys. Rev. A*, vol. 34, pp. 4025–4042, 1986.

[29] H. Wang, M. J. Freeman, and D. G. Steel, "Squeezed light from injection-locked quantum well lasers," *Phys. Rev. Lett.*, vol. 71, pp. 3951–3954, 1993.

[30] A. E. Siegman, *Lasers*, 1st ed. Sausalito, CA, USA: Univ. Sci. Books, 1986.

[31] M. AlMulla and J.-M. Liu, "Effects of the gain saturation factor on the nonlinear dynamics of optically injected semiconductor lasers," *IEEE J. Quantum Electron.*, vol. 50, no. 3, pp. 158–165, Mar. 2014.

[32] G. P. Agrawal, "Effect of gain and index nonlinearities on single-mode dynamics in semiconductor lasers," *IEEE J. Quantum Electron.*, vol. 26, no. 11, pp. 1901–1910, Nov. 1990.

[33] C.-H. Lin, H.-H. Lin, and F.-Y. Lin, "Four-wave mixing analysis of quantum dot semiconductor lasers for linewidth enhancement factor extraction," *Opt. Exp.*, vol. 20, pp. 101–109, 2012.

[34] B. Lingnau, K. Lüdge, W. W. Chow, and E. Schöll, "Failure of the α factor in describing dynamical instabilities and chaos in quantum-dot lasers," *Phys. Rev. E*, vol. 86, p. 065201(R), 2012.

[35] S. Wieczorek, T. B. Simpson, B. Krauskopf, and D. Lenstra, "Global quantitative predictions of complex laser dynamics," *Phys. Rev. E*, vol. 65, p. 045207, 2002.

[36] "Calculations with different laser dynamics parameters showed that the SNLC bifurcation does not always end where the P1 minimum matches the SNLC frequency, but typically the two values are similar. the P1 minimum can be pulled to terminate in nearby regions of P2 or aperiodic dynamics."

[37] S. K. Hwang, and D. H. Liang, "Effects of linewidth enhancement factor on period-one oscillations of optically injected semiconductor lasers," *Appl. Phys. Lett.*, vol. 89, pp. 061120-1–061120-3, 2006.

[38] T. B. Simpson, J.-M. Liu, and A. Gavrielides, "Small-signal analysis of modulation characteristics in a semiconductor laser subject to strong optical injection," *IEEE J. Quantum Electron.*, vol. 32, no. 8, pp. 1456–1468, Aug. 1996.

[39] L. G. Villanueva, E. KLenig, R. B. Karabalin, M. H. Matheny, R. Lifshitz, M. C. Cross, and M. L. Roukes, "Surpassing fundamental limits in oscillators using nonlinear resonators," *Phys. Rev. Lett.*, vol. 110, p. 177208, 2014.

Authors' photographs and biographies not available at the time of publication.